bio-protocol

Published: Apr 05, 2022

In vivo Ca^{2+} Imaging in Mouse Salivary Glands

Takahiro Takano* and David I. Yule

Department of Pharmacology and Physiology, University of Rochester, Rochester, NY, USA
*For correspondence: Takahiro_takano@urmc.rochester.edu

Abstract

Changes in intracellular calcium drive exocrine cell activity. In the salivary gland, acetylcholine released from parasympathetic neurons mobilizes endoplasmic reticulum calcium stores in acinar cells, which consequently initiates saliva secretion. However, our understanding of the signaling cascade is mainly based on *ex vivo* studies performed in enzymatically isolated cells. The dissociation process likely disrupts the extracellular matrix, removes neurons as the source of signal input, and disturbs the integrity of tight and gap junctional acinar connections. These alterations may affect the spatiotemporal properties of calcium signaling events. *In vivo* observations of calcium signals, where tissue organization is intact, are therefore important to establish the characteristics of physiological calcium signals that are crucial for the stimulation of fluid secretion. Here, we present a detailed protocol for *in vivo* imaging of calcium signaling events, following nervous stimulation by multi-photon microscopy in mouse salivary gland acinar cells, expressing the genetically encoded calcium indicator GCamp6F.

Keywords: Calcium, Exocrine acinar cells, Two-photon microscopy, Intravital imaging, Mouse, GCamp6F

This protocol was validated in: eLife (2021), DOI: 10.7554/eLife.66170

Background

Exocrine cells in the salivary gland secrete saliva, which is important for the initial stages of digestion and for the overall health of the oral cavity (Pedersen *et al.*, 2002). This is most clearly appreciated in disease states, including Sjogren's syndrome, and following γ-irradiation treatment of head and neck cancers, which result in salivary hypofunction. These patients experience difficulty speaking, chewing and swallowing food, and are susceptible to oral infections (Melvin, 1991). Fluid secretion is mainly driven by parasympathetic nerve input with local release of acetylcholine (ACh), which causes an elevation in cytosolic [Ca^{2+}] in acinar cells, through the activation of muscarinic receptors localized in the basal plasma membrane (PM) (**Figure 1A**) (Putney, 1982; Weiss *et al.*, 1982; Gallacher and Petersen, 1983; Matsui *et al.*, 2000; Ambudkar, 2011, 2016). Subsequent production of inositol 1,4,5 trisphosphate (IP_3) in the acinar cells follows, and results in activation of IP_3 receptors (IP_3R), that drives Ca^{2+} release from endoplasmic reticulum (ER) stores into the cytosolic space (Lee *et al.*, 1997; Futatsugi *et al.*, 2005; Pages *et al.*, 2019). The depletion of ER Ca^{2+} stores is in turn sensed by stromal interaction molecule 1, which undergoes a conformational change, aggregates, and gates the Ca^{2+} channel Orai 1 in the PM to open, which provides a sustained [Ca^{2+}] elevation.

To stimulate saliva flow, the primary effector of the increase in [Ca^{2+}] are TMEM16a channels localized in the apical PM facing the ductal lumen (Arreola *et al.*, 1996a, 1996b; Begenisich and Melvin, 1998; Romanenko *et al.*, 2010a).

The majority of type-2/3 IP_3Rs, which initiate the [Ca^{2+}] increase, are localized in the ER, in close apposition to TMEM16a (Lee *et al.*, 1997; Pages *et al.*, 2019). This spatial arrangement of IP_3R and TMEM16a suggests that the critical Ca^{2+} signaling event is restricted to the apical aspects of the cell. However, as Cl^- moves across the apical membrane, the activity of K channels is also increased, to maintain the membrane potential in favor of Cl^- exit. The K^+ channels are thought to be localized predominantly at the basolateral PM, and are also activated by the [Ca^{2+}] increase (Maruyama *et al.*, 1983; Nakamoto *et al.*, 2008, 2007; Romanenko *et al.*, 2007, 2010b). Indeed, *in vitro* observations using enzymatically dissociated acinar cells demonstrated that Ca^{2+} signaling is initiated at the apical pole, then spreads as a Ca^{2+} wave to the rest of the cell, delivering the signal to the basolateral side, presumably by Ca^{2+}-induced Ca^{2+} release through ryanodine receptors (Won *et al.*, 2007). These observations led to the development of a widely accepted model for how Ca^{2+} signals control exocrine secretion. Nevertheless, several caveats apply to this interpretation.

First, mechanical and enzymatic dissociation likely disrupts the extracellular matrix, the organization of PM-associated proteins, and the integrity of cellular junctions and connections. Second, isolation of acinar cells may also disrupt the cytoskeleton and the intracellular organization of organelles, which could all conceivably alter the spatio-temporal characteristics of Ca^{2+} signaling events. Further, stimulation of the cells is often *via* a constant bath application of a synthetic ligand designed to activate a specific receptor, which is quite different from physiological activation, where pulsatile release of neurotransmitters from terminals of axons embedded in the organ initiates the signal event. Furthermore, *in vivo*, neuronal input to individual acinar cells is likely heterogeneous, leading to variability in the response of particular cells, which is not reproduced by bath application of agonist. Therefore, the goal of this protocol is to provide a guide to facilitate observation of Ca^{2+} signaling within the intact salivary gland in a live animal, following physiological nervous input (**Figure 1A**) (Takano *et al.*, 2021).

Materials and Reagents

A. Animals

1. GCaMP6f^{flox} mice (Jackson Laboratory, catalog number: 028865)
2. Mist1^{CreERT2} (Jackson Laboratory, catalog number: 029228)

B. Materials

1. 1 mL syringe (BD Biosciences, catalog number: 309659)
2. 27 G needle (BD Biosciences, catalog number: 305109)
3. Feeding tubes (Instech, catalog number: FTP-22-25)

4. Mouse restrainer/stage (Custom-made by 3D printer, **Figure 1A**)
5. Gland holder (Custom-made by 3D printer, **Figure 1A**)
6. Tungsten wire, 0.125 mm (WPI, catalog number: TGW0515)
7. Cover glass, 18 mm diameter (Fisherbrand, catalog number: 12-545-100)
8. Hand warmer (Kobayashi Consumer Products, Hothands)
9. Cotton sponge (Covidien, Curity 9022)

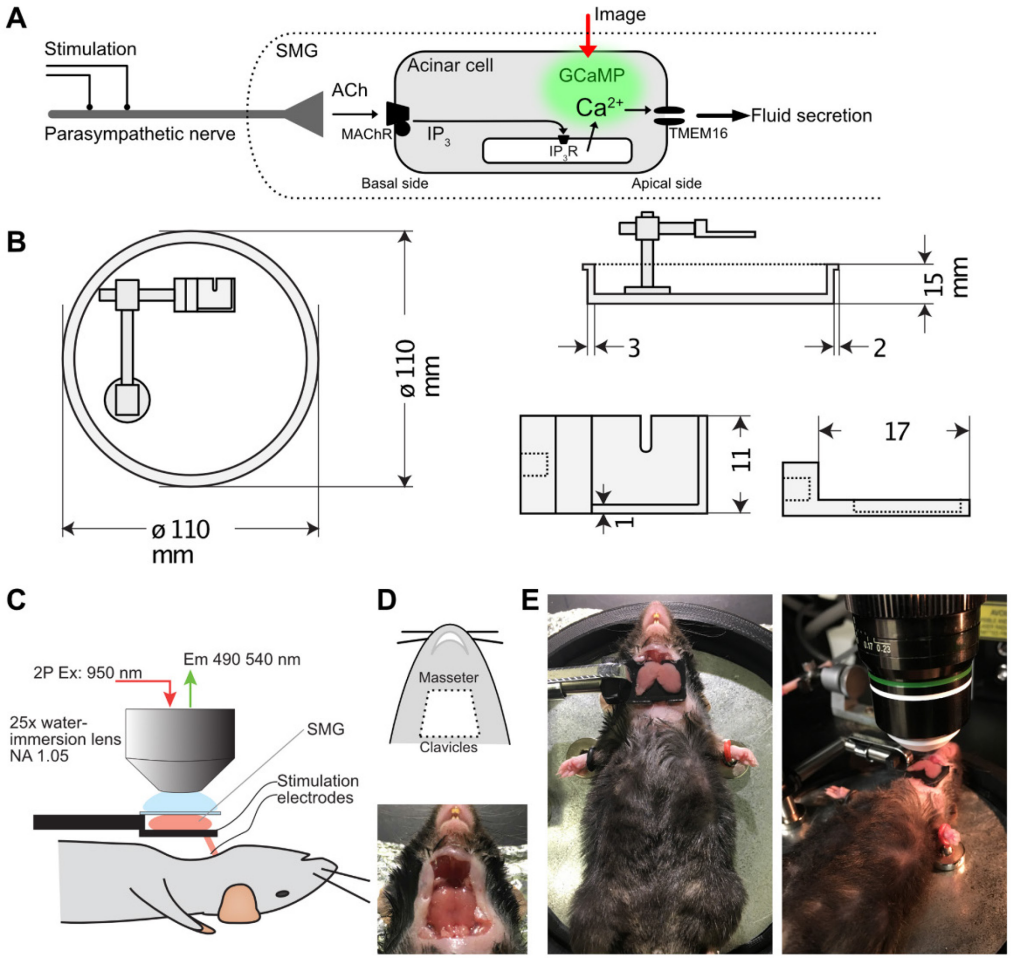

Figure 1. Design of *in vivo* salivary gland imaging setup.
A. A cartoon depicting calcium signaling in acinar cells of the salivary gland. Neuronal input and acinar cell architecture are preserved only *in vivo*. Nerve input can be electrically initiated, and acinar calcium signaling optically observed in real time with the genetically-encoded calcium probe GCaMP6F. **B.** Design diagrams of the animal restrainer stage and gland holder. **C.** A diagram of the 2-photon imaging arrangement. **D.** Position of skin incision and a photograph of the exposed submandibular gland (SMG). **E.** Photographs of the SMG placed on a holder, with a cover glass flattening its surface, and an objective lens situated on top of the gland.

C. Reagents

1. Tamoxifen (Sigma-Aldrich, catalog number: T5648)
2. Corn Oil (Sigma-Aldrich, catalog number: C8267)
3. Ketamine (Hospira, Ketamine HCl, NDC 0409-2051-15)
4. Xylazine (Akorn Animal Health, AnaSed, NDC 59399-110-20)
5. Hank's salt solution with calcium and magnesium, no phenol red (Gibco, catalog number: 14025-092)

6. Hair remover (Church & Dwight, Nair)
7. Ethanol, 200 proof (Koptec, V1001)
8. Petroleum jelly (Unilever, Vaseline)
9. Tamoxifen stock solution (see Recipes)
10. Salivary gland holder (see Recipes)

Equipment

1. Stereo microscope (LW Scientific, Z4)
2. Surgical scissors (Fine Science Tools, catalog number: 91460-11)
3. Forceps (Fine Science Tools, catalog number: 11252-40)
4. Two-photon laser-scanning microscope (Olympus, FVMPE-RS)
5. 25× water-immersion objective lens (Olympus, XLPlan NA 1.05 W MP)
6. Ti:Sapphire laser (Spectra-Physics, Insight X3)
7. Objective lens heater (OKOLab COL2532)
8. Stimulus Isolator (A.M.P.I., Iso-flex)
9. Pulse generator (Digitimer Ltd, DG2A)

Software

1. FV31s-SW (Olympus, FV31s-SW)
2. FIJI/ImageJ (NIH, https://imagej.net/software/fiji/)
3. Prism (GraphPad)

Procedure

A. Generation of mice expressing GCaMP6f in exocrine acinar cells

1. To generate Mist1$^{+/-}$;GCaMP6f$^{+/-}$ transgenic mice, cross 2–7 months old female homozygous GCaMP6f^{flox} mice (Jackson Laboratory; 028865) with 2–9 months old male heterozygous Mist1^{CreERT2} (Jackson Laboratory; 029228). Genotyping was carried out according to protocols supplied by the Jackson Laboratory (Genotyping protocols 27076 and 20626, respectively).
2. To induce GCaMP expression in acinar cells, treat Mist1$^{+/-}$;GCaMP6f$^{+/-}$ mice at least 6 weeks old with tamoxifen. Prepare 60 mg/mL tamoxifen in corn oil, and administer 0.25 mg/g body weight by oral gavage once a day for three consecutive days, using a plastic feeding tube attached to a 1 mL syringe. Imaging is carried out 1–4 weeks after the last tamoxifen administration.

B. Animal preparation

1. Anesthetize the animal with Ketamine [80 mg/kg body weight, intraperitonially (i.p.)] and Xylazine (10 mg/kg body weight, i.p.). Place the animal on a custom-made mouse-restrainer with the ventral side up (**Figure 1C–E**). Place a heat pad (HotHands, Kobayashi) under the restrainer and wrap the animal's body with a cotton sheet, to prevent hypothermia. Perform a toe-pinch intermittently, at least every 10–20 min, to evaluate the depth of anesthesia. Additional anesthetic of 20–40 mg/kg ketamine, is given when necessary.
2. To remove hair at the surgical region, apply hair remover cream to the animal's neck, then wipe with 70% ethanol. With a pair of scissors, make an incision at the neck just anterior to the clavicles, through the end of the masseter muscle (**Figure 1D**). Lift the incised skin to expose the submandibular/sublingual glands. Carefully tease away connective tissues surrounding the gland using two pairs of forceps, until the gland is detached from the body, except by a bundle composed of blood vessels, nerve, and the secretory duct, at the anterior side of the gland (**Figures 1C–E**).
3. Lift the gland and insert a pair of tungsten wires to the bundle, one at the base near the body, and the other

at where the bundle is connected to the gland. Connect the other ends of the wires to the stimulator.

4. Place the gland on a 11 × 17 mm custom build small holder situated directly above the neck, so that the position of the gland is not influenced by movement as a result of breathing (**Figure 1C, 1E**). Apply Hanks salt solution in the holder, apply petroleum jelly or silicone gel at the edge of the holder, then place a cover glass onto the gland, so that the surface of the gland is flattened, but the gland is not overtly squeezed by pressure.

C. *In vivo* imaging

1. Attach an objective heater to the 25× water immersion lens prior to the imaging session, to equilibrate the lens temperature to 37°C. Tune the excitation laser connected to an upright microscope at 950 nm. Set the emission filter at 495–540 nm.
2. Place the animal on the microscope stage. Apply Hank's solution between the objective lens and the cover glass holding the gland. Turn on a gooseneck light source and adjust the focus in bright field view through eyepieces. Find a flat clean region of the submandibular gland for imaging. Connect the stimulator to the pulse generator. Turn off the light source and keep the microscope stage dark, by covering the microscope with a black curtain and keeping the room dark. Set the resonance scanner of the FV31s-SW laser-scanning system to 30 frames per second, and collect an average of 3 frames as a single frame, to achieve a 10 fps image collection rate. The image resolution is 512 × 512 pixels, and the magnification is adjusted by zooming with scanner control, typically from 2× to 4× zoom.
3. Adjust the laser power so that the baseline fluorescence is faintly visible, about 20% of saturation (**Figure 2A**). PMT settings are fixed at 600 V, 1× gain, and 3% black level. Find the surface of that gland by moving focus, and set the registered depth as 0 µm. We typically image at depths between 10 and 55 µm from the surface of the gland. Adjust the laser power as depth changes.
4. A test time-course set of images is taken for 30 s without external stimulation. Acinar cell fluorescence should be stable without spontaneous flickering, and the imaging field should not drift in XY or Z directions.
5. Start the image collection set from 30 s to 5 min. During the image collection, deliver a train of electrical stimulation using a stimulus isolator set at 5 mA for 200 µs, controlled by a pulse generator set to 1–10 Hz, for 12 s up to 5 min (**Figure 2A**). After a series of images are captured, allow 1–5 min of resting time before the next image capture, to let the tissue fully recover from the stimulation applied.
6. For line scan imaging, find an acinar cell cluster that is orientated in the image plane, such that apical and basal sides of the acinar cell are clearly identified, and the imaging plane depth crosses near the center of the cell (**Figure 3A**). After the capture of a single image of a chosen field, a line is drawn in the image from the apical end, passing through the nucleus, to the basal aspect of an acinar cell. The scanning speed of the line varies according to the length of the line, and is typically 1–1.6 ms per line (**Figure 3B**).
7. Continue to perform a toe-pinch intermittently, at every 10–20 min, to evaluate the depth of anesthesia. Additional anesthetics of 20–40 mg/kg ketamine is given when necessary. Otherwise, administer 0.1 mL of saline solution every 30 min, to prevent dehydration. After the imaging, the animals are euthanized under anesthesia, according to a procedure approved by the University Committee on Animal Resources.

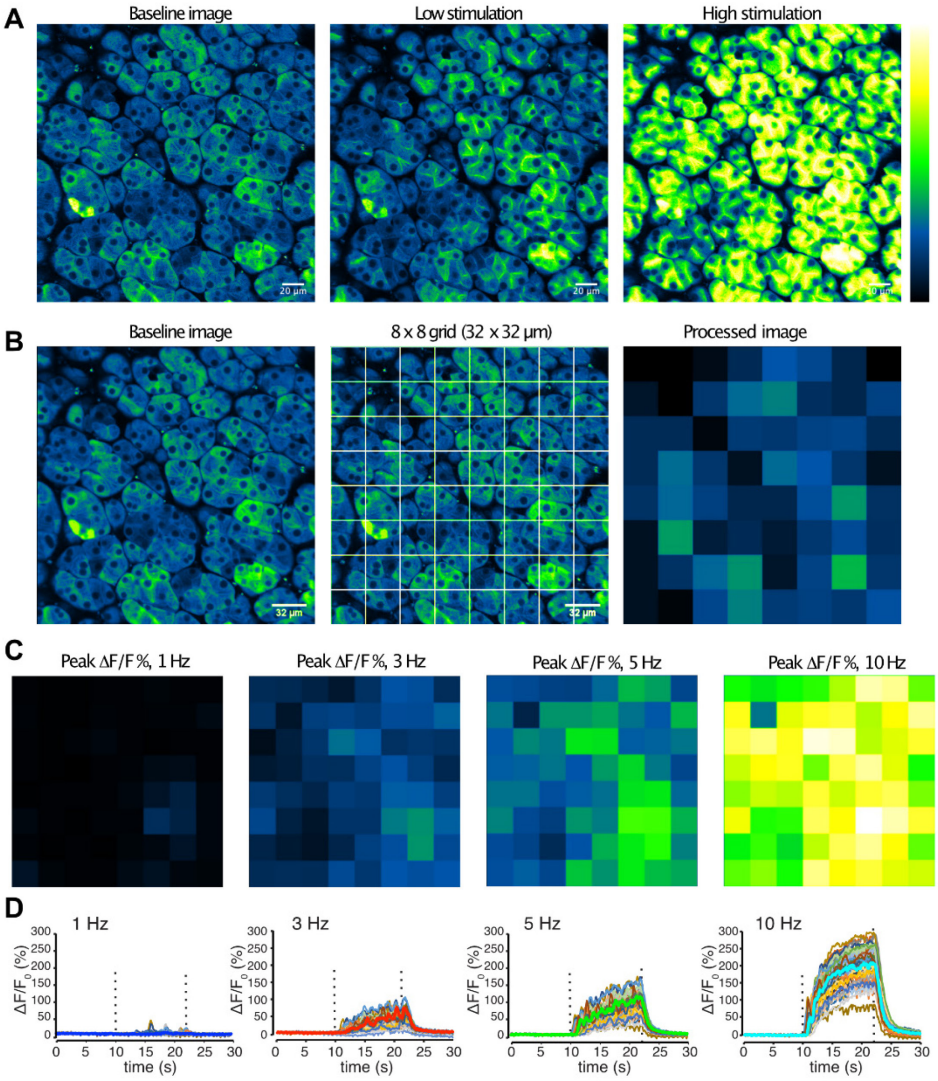

Figure 2. Image analyses of *in vivo* salivary gland imaging.

A. Images of acinar cells in submandibular gland before, and during low (3 Hz), or high (10 Hz) stimulations. **B.** Post-processing for spatio-temporal patterns of Ca^{2+} by nerve input. The image was subdivided into 8 × 8 grids, and average fluorescence intensity was obtained for each grid. **C–D**. Grid-analyses of an imaging field responding to 1–10 Hz stimulation. Grid images showing peak intensities (**C**) and time-course plots. Stimulation at the indicated frequency was applied between 10–22 s (**D**).

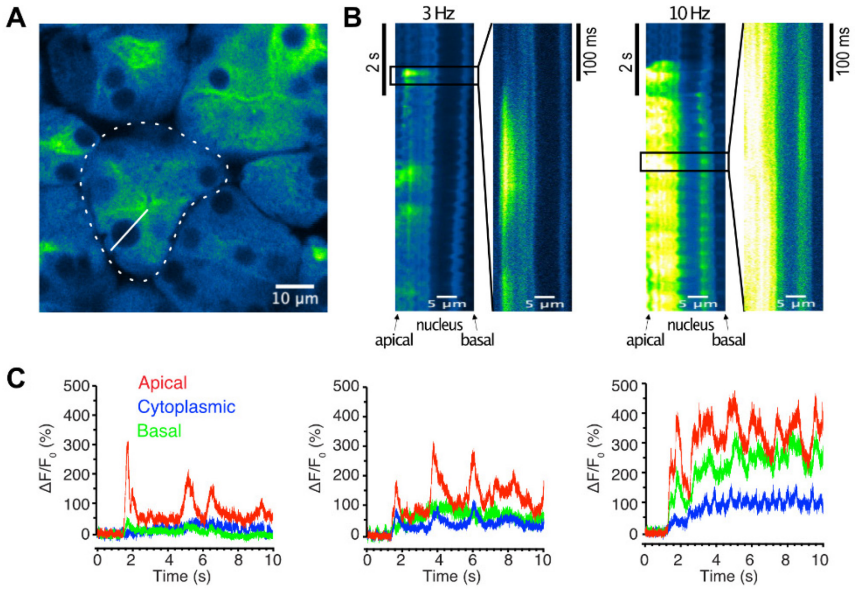

Figure 3. Image analyses of line-scan salivary gland imaging.
A. An image of a lobule showing radial arrangement of acinar cells, with the apical side at the center and the basal side at the circumference (dotted line). A line was defined in a cell from the apical end through the nucleus until the basal end (solid line). **B.** Line scan images across an acinar cell during 3 or 10 Hz stimulation, showing localization of Ca^{2+} at the apical side of the cell without intracellular Ca^{2+} spread toward the basal side. **C.** Time-course plots from regions of interest (ROI's) representing the apical (red), cytoplasmic (blue), and basal (green) regions, responding to 3 Hz (left panel), 5 Hz (middle panel), and 10 Hz (right panel) stimulations.

Data analysis

1. Open the acquired image in FIJI/ImageJ. Stimulation may cause mild drifting of the imaging field in the XY direction, so that the image series may have to be realigned to keep the cells in stationary positions throughout the time-course. For this, apply a descriptor-based series registration plugin (by Stephan Preibisch, included in the FIJI package) using the nucleus, appearing as blank fixed-size round spots, as references for positioning.
2. For whole field average Ca^{2+} changes over time, select the whole image using the ROI Manager, and measure mean gray values for each frame with the Multi Measure function. An average of gray values in frames before stimulation serves as the baseline value (F_0), and $\%\Delta F/F_0$ $[(F- F_0)/ F_0 \times 100]$ is then calculated for all the frames in a series. The standard deviation (SD) of the 100 baseline frames from grids in each image series provides an estimate of the noise level. A change >4 SD from the F_0 value is considered as an evoked Ca^{2+} signal.
3. For analyses of heterogeneity of Ca^{2+} responses in acinar cells stimulated in an imaging field, rather than manually identify each cell, whose sizes and shapes vary greatly, and whose cell boundaries are not always apparent, we divide the field into 8 x 8 grids. This yields 64 ROIs, which correspond to dimension of 32 × 32 μm^2 for images taken with a 25× objective, 512 × 512 pixel size, with zoom 2× (**Figure 2B**). The average intensity of each ROI grid is generated for each frame. The average of the first 100 frames prior to stimulation serves as baseline fluorescence (F_0), and $\%\Delta F/F_0$ $[(F- F_0)/F_0 \times 100]$ is calculated, using the Image calculator function, so that the converted 32-bit image series represents $[Ca^{2+}]$ changes over time expressed as $\%\Delta F/F_0$ in 8 × 8 alley of grids in the XY dimension (**Figures 2B–D**). Of note, we confirmed the validity of this analysis scheme by comparing information obtained from 8 × 8 grids to 16 × 16 grids, and randomly and manually selected individual acinar cells. Each scheme produced essentially equivalent data.
4. The percentage of acinar calls responding to a particular stimulation frequency is evaluated by counting the numbers of grids that showed at least one response above the noise level during the stimulation duration. To

calculate the latency prior to a measurable response, the time to the first observed Ca^{2+} signal that meets the criteria as responding after the initiation of the stimulation are recorded. Non-responding grids are excluded from the latency analysis. Peak Ca^{2+} amplitude is obtained by extracting maximum $\%\Delta F/F_0$ values during the stimulation duration from each grid.

5. For XT-line scan images, we separate the line into three zones, to represent the basal, cytosolic, and apical regions. The line contains the nucleus, which appears as a dark band near the basal side, and this band separates the basal region from the cytosolic and apical regions (**Figure 3A, 3B**). Each region is defined as a 3 μm wide line within the image, and fluorescent intensity before stimulation for each region serves as the baseline intensity ($F_0 = 0\%$) (**Figure 3C**).
6. All statistical analyses are performed with paired t test, one-way ANOVA, and linear regression, using Prism (GraphPad).

Recipes

1. Tamoxifen stock solution
   Tamoxifen powder: 600 mg
   Corn oil: 10 mL
   Heat to 70°C until dissolved.
2. Salivary gland holder
   Thorlabs, ER1 Assembly rods, ×3
   Thorlabs, ER90B angle clamps, ×2
   Permanent Magnet, Round, ½" diameter
   Holder tray, made with 3D printer

Acknowledgments

We thank Dr. Catherine Ovitt, University of Rochester, for providing $Mist1^{CreERT2}$ mice, Multiphoton and Analytical Imaging Center for providing Olympus FV31s-SW multiphoton system, and our laboratory members for valuable input and help. This work was supported by NIH grants RO1DE019245 and RO1DE014756. Research using this protocol was published in Takano *et al.* (2021; doi: 10.7554/eLife.66170).

Competing interests

The authors declare no conflicts of interest.

References

Ambudkar, I. S. (2011). Dissection of calcium signaling events in exocrine secretion. *Neurochem Res* 36(7): 1212-1221.

Ambudkar, I. S. (2016). Calcium signalling in salivary gland physiology and dysfunction. *J Physiol* 594(11): 2813-2824.

Arreola, J., Melvin, J. E. and Begenisich, T. (1996a). Activation of calcium-dependent chloride channels in rat parotid acinar cells. *J Gen Physiol* 108(1): 35-47.

Arreola, J., Park, K., Melvin, J. E. and Begenisich, T. (1996b). Three distinct chloride channels control anion movements in rat parotid acinar cells. *J Physiol* 490 (Pt 2): 351-362.

Begenisich, T. and Melvin, J. E. (1998). Regulation of chloride channels in secretory epithelia. *J Membr Biol* 163(2):

77-85.

Futatsugi, A., Nakamura, T., Yamada, M. K., Ebisui, E., Nakamura, K., Uchida, K., Kitaguchi, T., Takahashi-Iwanaga, H., Noda, T., Aruga, J. and Mikoshiba, K. (2005). IP3 receptor types 2 and 3 mediate exocrine secretion underlying energy metabolism. *Science* 309(5744): 2232-2234.

Gallacher, D. V. and Petersen, O. H. (1983). Stimulus-secretion coupling in mammalian salivary glands. *Int Rev Physiol* 28: 1-52.

Lee, M. G., Xu, X., Zeng, W., Diaz, J., Wojcikiewicz, R. J., Kuo, T. H., Wuytack, F., Racymaekers, L. and Muallem, S. (1997). Polarized expression of Ca^{2+} channels in pancreatic and salivary gland cells. Correlation with initiation and propagation of $[Ca^{2+}]_i$ waves. *J Biol Chem* 272(25): 15765-15770.

Maruyama, Y., Gallacher, D. V. and Petersen, O. H. (1983). Voltage and Ca^{2+}-activated K^+ channel in baso-lateral acinar cell membranes of mammalian salivary glands. *Nature* 302(5911): 827-829.

Matsui, M., Motomura, D., Karasawa, H., Fujikawa, T., Jiang, J., Komiya, Y., Takahashi, S. and Taketo, M. M. (2000). Multiple functional defects in peripheral autonomic organs in mice lacking muscarinic acetylcholine receptor gene for the M3 subtype. *Proc Natl Acad Sci U S A* 97(17): 9579-9584.

Melvin, J. E. (1991). Saliva and dental diseases. *Curr Opin Dent* 1(6): 795-801.

Nakamoto, T., Romanenko, V. G., Takahashi, A., Begenisich, T. and Melvin, J. E. (2008). Apical maxi-K (KCa1.1) channels mediate K^+ secretion by the mouse submandibular exocrine gland. *Am J Physiol Cell Physiol* 294(3): C810-819.

Nakamoto, T., Srivastava, A., Romanenko, V. G., Ovitt, C. E., Perez-Cornejo, P., Arreola, J., Begenisich, T. and Melvin, J. E. (2007). Functional and molecular characterization of the fluid secretion mechanism in human parotid acinar cells. *Am J Physiol Regul Integr Comp Physiol* 292(6): R2380-2390.

Pages, N., Vera-Siguenza, E., Rugis, J., Kirk, V., Yule, D. I. and Sneyd, J. (2019). A Model of [Formula: see text] Dynamics in an Accurate Reconstruction of Parotid Acinar Cells. *Bull Math Biol* 81(5): 1394-1426.

Pedersen, A. M., Bardow, A., Jensen, S. B. and Nauntofte, B. (2002). Saliva and gastrointestinal functions of taste, mastication, swallowing and digestion. *Oral Dis* 8(3): 117-129.

Putney, J. W., Jr. (1982). Cellular regulation. *Science* 216(4553): 1403-1404.

Romanenko, V. G., Catalan, M. A., Brown, D. A., Putzier, I., Hartzell, H. C., Marmorstein, A. D., Gonzalez-Begne, M., Rock, J. R., Harfe, B. D. and Melvin, J. E. (2010a). Tmem16A encodes the Ca^{2+}-activated Cl^- channel in mouse submandibular salivary gland acinar cells. *J Biol Chem* 285(17): 12990-13001.

Romanenko, V. G., Nakamoto, T., Srivastava, A., Begenisich, T. and Melvin, J. E. (2007). Regulation of membrane potential and fluid secretion by Ca^{2+}-activated K^+ channels in mouse submandibular glands. *J Physiol* 581(Pt 2): 801-817.

Romanenko, V. G., Thompson, J. and Begenisich, T. (2010b). Ca^{2+}-activated K channels in parotid acinar cells: The functional basis for the hyperpolarized activation of BK channels. *Channels (Austin)* 4(4): 278-288.

Takano, T., Wahl, A. M., Huang, K. T., Narita, T., Rugis, J., Sneyd, J. and Yule, D. I. (2021). Highly localized intracellular Ca^{2+} signals promote optimal salivary gland fluid secretion. *Elife* 10: e66170.

Weiss, S. J., McKinney, J. S. and Putney, J. W., Jr. (1982). Regulation of phosphatidate synthesis by secretagogues in parotid acinar cells. *Biochem J* 204(2): 587-592.

Won, J. H., Cottrell, W. J., Foster, T. H. and Yule, D. I. (2007). Ca^{2+} release dynamics in parotid and pancreatic exocrine acinar cells evoked by spatially limited flash photolysis. *Am J Physiol Gastrointest Liver Physiol* 293(6): G1166-1177.